Proton Release Group of *pharaonis* Phoborhodopsin Revealed by ATR-FTIR Spectroscopy[†]

Yuya Kitade,[‡] Yuji Furutani,[‡] Naoki Kamo,[§] and Hideki Kandori*[,‡]

Department of Frontier Materials, Nagoya Institute of Technology, Showa-ku, Nagoya 466-8555, Japan, and Graduate School of Pharmaceutical Sciences, Hokkaido University, Sapporo 060-0810, Japan

Received October 22, 2008; Revised Manuscript Received January 7, 2009

ABSTRACT: The proton release mechanism has been one of the recent interesting topics in the field of microbial rhodopsins since it was established that a protonated water cluster is the proton release group (PRG) in bacteriorhodopsin (BR). *pharaonis* phoborhodopsin [*p*pR, also called *pharaonis* sensory rhodopsin II (*p*SRII)] is a photoreceptor for negative phototaxis in *Natronomonas pharaonis*, and in the absence of transducer protein, *p*HtrII, *p*pR can pump protons like BR. Fast, BR-like proton release was observed during the lifetime of the M intermediate (ppR_M) at low pH, but it was slowed in the absence of Cl^- [Iwamoto, M., et al. (2004) *Biochemistry 43*, 3195]. This observation suggests that Cl^- binding controls the pK_a of PRG in *p*pR and ppR_M. In this paper, we studied the molecular mechanism of the PRG action in *p*pR by means of Cl^--induced and light-induced difference attenuated total reflection (ATR) FTIR spectroscopy in the aqueous phase. Cl^--induced difference ATR-FTIR spectra clearly demonstrated that binding of Cl^- to *p*pR accompanies protonation of a carboxylic acid (C═O stretch at 1724 cm^{-1}). The amino acid was identified as Asp193, because the corresponding band is shifted to 1705 cm^{-1} in the D193E mutant protein. Light-induced ppR_M minus *p*pR difference ATR-FTIR spectra show the deprotonation signal of Asp193 (at 1724 cm^{-1}) only in the presence of Cl^-. The double-difference spectrum between the light-induced changes in the presence and absence of Cl^- is a mirror image of the spectrum of Cl^- binding in the dark, indicating that ppR_M formation accompanies deprotonation of Asp193 and dissociation of Cl^- simultaneously. It was also shown that structural changes of arginine are involved in these processes by use of [^{15}N]arginine-labeled *p*pR. We thus conclude that the PRG of *p*pR includes Asp193, whose pK_a changes are controlled by Cl^- and Arg72.

Proton transfer reactions play important role in cellular bioenergetics. One of the best understood proteins is bacteriorhodopsin (BR)[1] from *Halobacterium salinarum*, whose light-induced proton transfer reactions yield unidirectional transport of protons (*1, 2*). The first proton transfer takes place from the protonated Schiff base to Asp85 upon formation of the M intermediate, where an internal water molecule plays an important role (*3*−*5*). This reaction induces the release of a proton from the proton release group (PRG) to the extracellular side by lowering the pK_a value of the PRG from 9 to 5.8 at the M intermediate (*6*). Two glutamic acids at the extracellular surface, Glu204 and Glu194, were good candidates for the PRG, because their mutations significantly affect proton release (*7*−*9*). However, the deprotonation signal of carboxylic acid was not clearly detectable upon formation of the M intermediate (*10*−*12*), suggesting that the PRG is not formed by these glutamic acids. A new insight was gained from time-resolved FTIR studies by Gerwert and co-workers, which reported a broad negative IR continuum band at 2000−1800 cm^{-1} in the M-minus-BR difference spectrum (*10*). This observation indicates that the continuum vibration is only present in BR, but not in the M state, being consistent with what is expected from the vibration of the PRG. The continuum signal is significantly affected by mutations near the extracellular surface such as Tyr57, Arg82, Ser193, Glu194, and Glu204, and it was proposed that the continuum band originates from a protonated water cluster (*13*−*15*). Our recent time-resolved FTIR study of BR indeed observed an isotope effect of ^{18}O water on the continuum signal, indicating that the continuum band contains vibrations of water molecules (*16*). Thus, it is now established that the PRG in BR is a protonated water cluster, though the structure of the water cluster and mechanism of its high pK_a are still under investigation.

The PRG is not essential for the proton pumping machinery of BR, because BR can pump protons at pH <5.8 and >9, and several fast proton release-deficient mutants can pump protons as well (*3, 17, 18*). In these cases, fast proton release does not occur, but slower proton release occurs from Asp85 during the decay of the O intermediate. It should be noted, however, that the PRG is functionally important, because these fast release-defective proteins exhibit slow

[†] This work was supported by grants from Japanese Ministry of Education, Culture, Sports, Science, and Technology to H.K. (19370067, 20044012, and 20050015) and Y.F. (19042013 and 19045015).

* To whom correspondence should be addressed. Phone and fax: 81-52-735-5207. E-mail: kandori@nitech.ac.jp.

[‡] Nagoya Institute of Technology.

[§] Hokkaido University.

[1] Abbreviations: BR, bacteriorhodopsin; PRG, proton release group; *p*pR, *pharaonis* phoborhodopsin; *p*HtrII, *pharaonis* halobacterial transducer II; ATR, attenuated total reflection; FTIR, Fourier transform infrared; PC, L-α-phosphatidylcholine; HOOP, hydrogen out-of-plane.

10.1021/bi801984u CCC: $40.75
Published on Web 01/29/2009

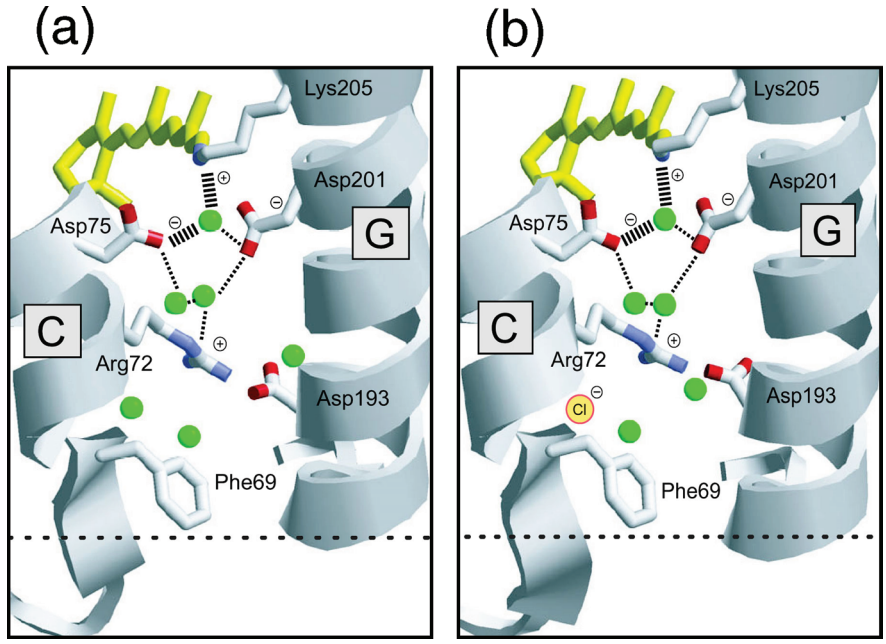

FIGURE 1: X-ray crystallographic structures of *pharaonis* phoborhodopsin (*p*pR) in the extracellular domain, which reported the absence [a (*27*)] or presence [b (*28*)] of the Cl^- binding site. The membrane normal is approximately in the vertical direction of this figure, and horizontal dotted lines represent the supposed boundary of the membrane. Dotted lines in the Schiff base region represent putative hydrogen bonds, where strong hydrogen bonds between the Schiff base and water and between water and Asp75 (thick dotted lines) are obtained from refs *46* and *47*, respectively. Interestingly, the structure of the extracellular domain is similar in the absence and presence of Cl^-. It appears that one of the water molecules in panel a is replaced by Cl^- in panel b.

photocycles. For instance, the photocycle of E204Q is ~30 times slower than that of the wild type, indicating that the efficiency of the proton pump is significantly lowered (*7*). Other proton-pumping proteins such as proteorhodopsin (PR) (*19*) and *Leptosphaeria* rhodopsin (LR) (*20*) exhibit no fast proton release, and this fact may suggest that BR has acquired PRG for efficient proton pumping during evolution.

pharaonis phoborhodopsin [*p*pR, also called *pharaonis* sensory rhodopsin II (*p*SRII)] is a negative phototaxis sensor in *Natronomonas pharaonis*, where *p*pR forms a 2:2 complex with its cognate transducer protein, *p*HtrII (*21*−*23*). In the absence of *p*HtrII, *p*pR pumps protons like BR (*24, 25*). Iwamoto et al. reported that *p*pR exhibits fast proton release at pH values between 5 and 8 in a Cl^--dependent manner (*26*). In the presence of Cl^-, *p*pR releases a proton before the M state decays (in the time range of 100 ms), followed by slower proton uptake (continued into the second time range) (*26*). In contrast, in the absence of Cl^-, fast proton release does not occur from *p*pR at any pH. Thus, the fast proton release is probably related to the binding of Cl^- in the extracellular region. Figure 1 shows the X-ray crystallographic structures of *p*pR from two different groups. While the overall structures are very similar, Cl^- binding was different between the two structures. Luecke et al. did not observe specific binding of Cl^- (Figure 1a) (*27*), but Royant et al. reported Cl^- binding near the extracellular surface (Figure 1b) (*28*). The difference presumably arose from experimental conditions for the preparation of the crystals, where Royant et al. crystallized *p*pR at higher salt concentrations. Interestingly, the two structures are very similar to each other (Figure 1), while spectroscopic measurements showed that the fast proton release occurs only in the presence of Cl^- (Figure 1b), but not in its absence (Figure 1a). Iwamoto et al. also showed that mutation of Asp193 inhibited fast proton release, suggesting that Asp193 is important for this process (*26*). According to the structure, Asp193 is located 6.3 Å from the bound Cl^- ion (Figure 1). This may suggest that Asp193 is a proton release group of *p*pR only in the presence of Cl^-, and the absence of proton release without Cl^- might originate from the deprotonated state of Asp193. However, there has been no direct experimental proof of the role of Cl^- in proton release by *p*pR.

In this work, we applied an attenuated total reflection (ATR) Fourier-transform infrared (FTIR) technique to investigate the fast proton release mechanism of *p*pR. FTIR spectroscopy is a powerful tool for understanding the molecular mechanism of rhodopsins in action, and we previously applied this technique to *p*pR (*29, 30*) and the *p*pR−*p*HtrII complex (*31, 32*). In these measurements, hydrated films were used, which allowed detailed spectral analysis, including that of a single water molecule bound to the protein. However, it is impossible to accurately control pH and salt conditions in hydrated film samples. In contrast, ATR-FTIR spectroscopy uses the sample in aqueous solution, where pH and ionic composition are accurately controlled. In addition, ligand binding and dissociation can be tested via ATR-FTIR spectroscopy, because the sample is surrounded by the aqueous phase (*33*−*35*). Recently, Jiang et al. introduced a further breakthrough by ATR-FTIR spectroscopy of *p*pR (*p*SRII), where difference spectra were measured upon voltage changes across the membrane (*36*). Thus, ATR-FTIR spectroscopy is a potentially powerful method for investigating the structure−function relationship in membrane proteins.

Here, we first measured spectral changes of *p*pR upon Cl^- binding by use of ATR-FTIR spectroscopy. This enabled us to conclude that Cl^- binding accompanies a proton uptake by Asp193 in the extracellular domain. Then, we measured light-induced M minus *p*pR difference spectra in the absence and presence of Cl^-. Interestingly, the double-difference

spectrum between the light-induced changes in the absence and presence of Cl^- is a mirror image of the spectrum of Cl^- binding to *p*pR in the dark. This implies that the formation of M accompanies release of Cl^- as well as release of a proton from Asp193. The molecular mechanism of the fast release of a proton from *p*pR and protein structural changes at the exctracellular domain are discussed on the basis of these observations.

MATERIALS AND METHODS

Preparation of ppR Samples. Expression and purification of histidine-tagged recombinant *p*pR, the wild-type and D193E mutant proteins, were performed as previously described (*29, 37*). Briefly, *p*pR proteins possessing a histidine tag at the C-terminus were expressed in *Escherichia coli* cells, solubilized with 1.5% *n*-dodecyl β-D-maltoside (DM), and purified by a Ni^{2+} column. The purified sample was then mixed with L-α-phosphatidylcholine (PC) in the presence of Bio-Beads (Bio-Rad, Hercules, CA), where the molar ratio of added PC to *p*pR was 30. [$\eta_{1,2}$-^{15}N]Arginine-labeled *p*pR was prepared similarly by the method described previously (*38*).

Perfusion-Induced ATR-FTIR Spectroscopy. The *p*pR sample was placed on the surface of diamond ATR crystal (SMITHS, nine effective internal reflections). After being dried in a gentle stream of N_2, the sample was rehydrated with perfusion buffer [50 mM citrate (pH 5)]. Before Cl^--induced difference spectra were recorded, the film was perfused with the same buffer at a flow rate of 0.6 mL/min for 100 min. ATR-FTIR spectra of the *p*pR film were recorded at 293 K and 2 cm^{-1} resolution with a Bio-Rad FTS-6000 spectrometer, equipped with a liquid nitrogen-cooled MCT detector. A background spectrum of the film (an average of 512 interferograms) was first recorded during perfusion with buffer in the absence of NaCl. The buffer was then switched to that containing 50 mM NaCl, and after a 2 min delay for equilibration, a Cl^- binding minus Cl^--free difference spectrum was recorded (an average of 512 interferograms). Then, after a new background was taken, the buffer was switched back to that without NaCl, and after a 3 min delay, an equivalent Cl^--free minus Cl^- binding difference spectrum was recorded. The cycling procedure was repeated 8−16 times, and the difference spectra were calculated as averages of *p*pR(Cl^-) minus *p*pR(free) spectra and *p*pR(free) minus *p*pR(Cl^-) spectra. The flow rate was maintained at 0.6 mL/min.

Light-Induced ATR-FTIR Spectroscopy. The *p*pR sample was placed on the surface of the diamond ATR crystal. After being dried in a gentle stream of N_2, the sample was rehydrated with perfusion buffer [50 mM citrate (pH 5)]. Before measurement, the film was perfused with the same buffer in the presence and absence of 400 mM NaCl at a flow rate of 0.6 mL/min for 100 min. The M intermediate was accumulated by illumination of each sample with a >500 nm light at 293 K. Difference infrared spectra at 293 K were recorded by subtracting the spectrum taken before illumination from that during illumination. Ninety-six independent measurements with 128 interferograms were averaged.

RESULTS

Structural Changes of ppR Induced by Chloride Binding. *p*pR-containing PC liposomes were first dried on an ATR diamond cell and were alternately perfused by Cl^--free or Cl^--containing buffer [50 mM NaCl and 50 mM citrate (pH 5.0)]. We confirmed that the *p*pR(Cl^-) minus *p*pR(free) spectra and *p*pR(free) minus *p*pR(Cl^-) spectra represent mirror images of each other, so that the measurements were repeated by changing buffers repeatedly. The solid line in Figure 2a shows the *p*pR(Cl^-) minus *p*pR(free) difference spectrum obtained in this way. It should be noted that this has spectral changes of water molecules and buffer components in addition to the spectral changes of *p*pR itself. Thus, we adopted the following correction to remove such spectral changes.[2]

First, we attempted to remove the contribution of water molecules. Dotted and dashed lines in Figure 2a represent difference spectra between Cl^--free and Cl^--containing buffers without sample (dotted line, 50 mM NaCl; dashed line, 4 M NaCl), where the dotted line consists of raw data but the dashed line was multiplied by 0.012 for normalization. These difference spectra originate from spectral changes in water molecules induced by binding of NaCl, as evidenced by a positive O−H bending vibrations at ∼1630 cm^{-1} and negative vibrations at 1000−800 cm^{-1}. By subtracting the contribution of water molecules, we obtained the difference spectrum shown in Figure 2b. It should be noted that the spectrum contains the signals of the buffer, as the different salt conditions (0 and 50 mM NaCl) appear to change the sample conditions, such as the thickness or density of the liposome layer adsorbed on the ATR crystal. The dotted line in Figure 2c represents the absolute spectrum of 2 M citrate (pH 5) after subtraction of the water contribution, which was then multiplied by −0.0045. Two strong peaks at 1577 and 1387 cm^{-1} originate from citrate, and from the two spectra in Figure 2c, we obtained the difference spectrum in Figure 2d. The present correction of the buffer contribution may not be quantitative, but peaks due to water molecules (dotted and dashed lines in Figure 2a) and the buffer (dotted line in Figure 2c) are broader than those originating from *p*pR (Figure 2d). In addition, important bands, such as a positive peak at 1724 cm^{-1}, are detectable even in the raw data (solid line in Figure 2a). Thus, it is safe to assume that the spectrum in Figure 2d represents the *p*pR(Cl^-) minus *p*pR(free) difference spectrum upon binding of Cl^- to *p*pR.

The *p*pR(Cl^-) minus *p*pR(free) difference spectrum in Figure 2d exhibits sharp peaks at 1724 (+), 1686 (−), 1671 (+), 1652 (−), 1619 (+), 1593 (−), 1542 (+), and 1526 (−) cm^{-1}. The specific Cl^- binding to *p*pR is also supported by the fact that these peaks were not observed in the measurements with SO_4^{2-}-containing buffer (data not shown). It should be noted that intense peaks were not observed in the 1500−800 cm^{-1} range, which includes the frequency region of fingerprint and HOOP vibrations of the retinal chromophore. This implies that Cl^- binding to *p*pR does not cause structural changes in the retinal chromophore. This is consistent with the previous observation that Cl^- does not affect the absorption of *p*pR (*39*). X-ray crystallography also

[2] Iwamoto et al. suggested the K_d of Cl^- binding is higher than 50 mM (*26*). Therefore, we first measured light-induced *p*pR$_M$ minus *p*pR difference spectra in the presence of 400 mM NaCl. On the other hand, a higher salt concentration yields larger spectral changes of water molecules and buffer components in the *p*pR(Cl^-) minus *p*pR(free) difference spectra in the dark. Thus, we obtained the *p*pR(Cl^-) minus *p*pR(free) spectra in the presence of 50 mM NaCl. Since the binding of Cl^- to the D193E mutant protein was weaker than that of the wild type, we used 100 mM NaCl for the measurement of D193E.

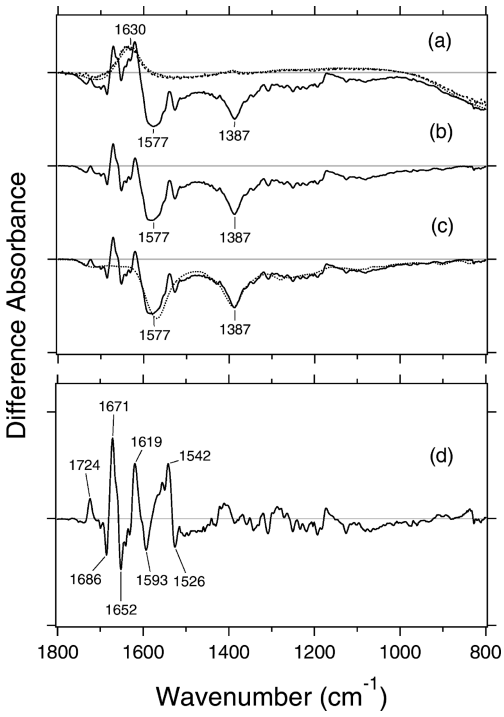

FIGURE 2: Difference ATR-FTIR spectra of the Cl^- binding to *p*pR at pH 5 and 293 K. (a) The solid line represents the difference spectrum for *p*pR between the presence and absence of Cl^- in the buffer (50 mM NaCl), where positive and negative signals correspond to Cl^--bound and Cl^--free forms, respectively. Dotted and dashed lines show the difference spectra measured under identical conditions without a *p*pR sample, where positive signals correspond to 50 mM and 4 M NaCl in the buffer, respectively. Dotted and dashed lines were multiplied by 1.0 and 0.012, respectively, for normalization. The broad spectral feature at 1700−1500 and 1000−800 cm^{-1} originates from infrared absorption of water. The dotted line was multiplied by 0.012 to show the flat curve at 1000−800 cm^{-1}. (b) Difference ATR-FTIR spectrum after subtraction of the water contribution, where the dashed line is subtracted from the solid one in panel a. (c) The solid line is from panel b, and the dotted line represents the absolute spectrum of 2 M citrate at pH 5 after being multiplied by −0.0045. (d) Difference ATR-FTIR spectrum of Cl^- binding to *p*pR at pH 5 and 293 K, where positive and negative signals correspond to Cl^--bound and Cl^--free forms, respectively. The spectrum is calculated by subtraction of the buffer contribution (dotted line in panel c) from the spectrum in panel c (solid line). The perfusion buffer for the *p*pR sample was 50 mM citrate (pH 5) with and whithout 50 mM NaCl. One division of the *y*-axis corresponds to 0.005 (a−c) and 0.002 (d) absorbance unit.

reported that the Cl^- binding site is located at the exctracellular domain distant from the retinal Schiff base (13.6 Å) (*28*), which is also consistent with the observation described here. This is in clear contrast to the Cl^- binding to halorhodopsin (*33*), where fingerprint and HOOP vibrations are affected.

The bands between 1700 and 1500 cm^{-1} possibly originate from amide I and amide II vibrations of the peptide backbone. The possible involvement of the C−N stretching vibration of arginine will be examined below by use of [^{15}N]arginine-labeled *p*pR. The positive peak at 1724 cm^{-1} is characteristic of protonated carboxylic acids, and the absence of the corresponding negative band at 1800−1700 cm^{-1} strongly suggests that binding of Cl^- to *p*pR accompanies protonation of a carboxylate. The corresponding negative signal for deprotonated carboxylate may appear at 1400−1350 cm^{-1} (symmetric COO^- stretching).

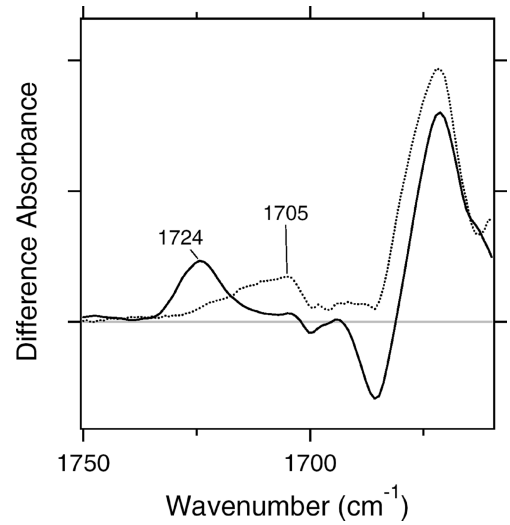

FIGURE 3: Difference infrared spectra between the Cl^--bound form and the Cl^--free form of *p*pR by ATR-FTIR spectroscopy at 293 K in the 1750−1660 cm^{-1} region. The negative side represents the Cl^--free form, and the positive side represents the Cl^--bound form. Solid and dotted lines represent the spectra for WT and D193E *p*pR, respectively. The perfusion buffer was 50 mM citrate (pH 5) with and whithout Cl^- (WT, 50 mM NaCl; D193E, 100 mM NaCl). The averaged spectra were multiplied by 1.0 (WT) and 1.7 (D193E) to normalize the spectral changes in the amide I region. One division of the *y*-axis corresponds to 0.001 absorbance unit.

Figure 3 compares the difference spectra induced by binding of Cl^- to *p*pR at 1750−1660 cm^{-1} between the wild-type (solid line) and the D193E mutant (dotted line) proteins. It appears that the spectrum of D193E lacks a negative 1686 cm^{-1} band (Figure 2d), while positive bands at 1671 and 1619 cm^{-1} were observed as well as the wild type (Figure 2b) (data not shown). Therefore, we normalized the two spectra by use of the amide I vibrations. Figure 3 clearly shows that the positive 1724 cm^{-1} band in the wild type shifts to 1705 cm^{-1} in D193E. We thus concluded that the 1724 cm^{-1} band originates from the C═O stretch of Asp193. It is likely that Cl^- binding accompanies protonation of Asp193 at the extracellular side. According to the X-ray crystal structure, the distance between Cl^- and Asp193 is 6.3 Å, indicating that no direct contact exists between them. However, the water-containing hydrogen bonding network may modulate the pK_a of Asp193 upon Cl^- binding. Figure 1a shows the presence of two positive (the Schiff base and Arg72) and three negative (Asp75, Asp201, and Asp193) charges in the extracellular domain of *p*pR. Two positive and three negative charges are probably preserved in *p*pR(Cl^-), where Cl^- replaces Asp193. In other words, "Cl^- binding" actually indicates the binding of H^+ and Cl^- to the protein.

Structural Changes in the M Intermediates. Figure 4a exhibits a spectral comparison of the M minus *p*pR difference spectra in the absence (dotted line) and presence (solid line) of 400 mM NaCl at 293 K. The dotted line coincides well with the reported M minus *p*pR difference spectrum of the hydrated film (*30, 39*), indicating that hydrated film conditions are similar to those in the aqueous phase. The detailed spectral comparison of *p*pR and the *p*pR−*p*HtrII complex in hydrated films (transmission FTIR) and aqueous solution (ATR-FTIR) will be described elsewhere.

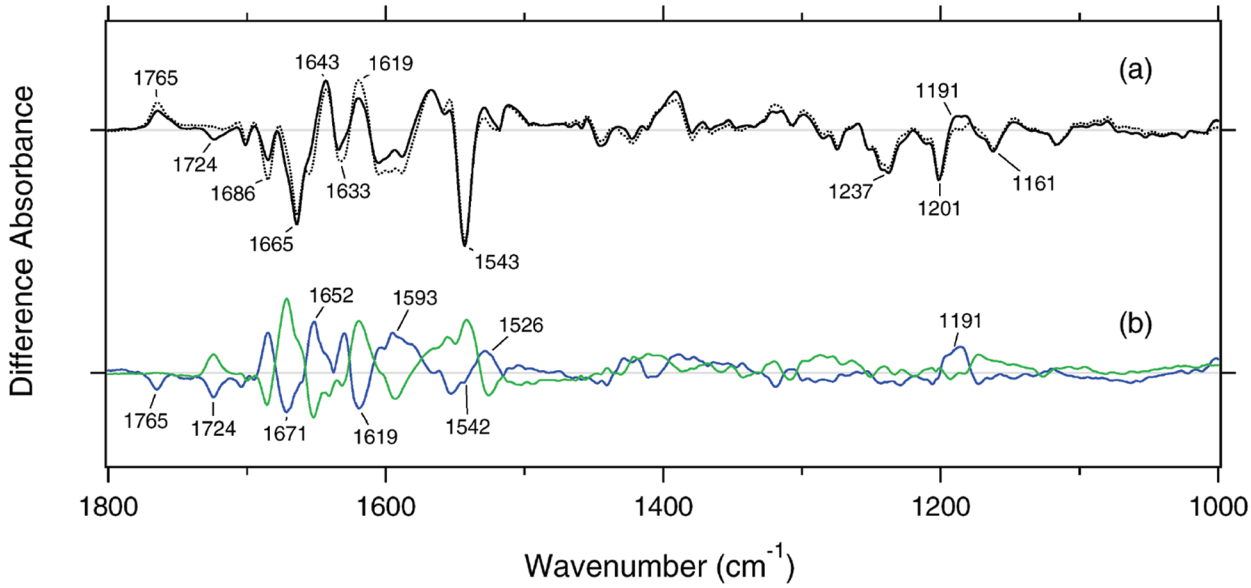

FIGURE 4: (a) M minus *p*pR difference spectra determined by ATR-FTIR spectroscopy at 293 K in the 1800−1000 cm^{-1} region. Solid and dotted lines represent the spectra in the presence and absence of Cl^- (400 mM NaCl), respectively. The averaged spectra were multiplied by 1.0 (without NaCl) and 1.65 (with 400 mM NaCl) to show the same amplitudes for the negative bands at 1543 and 1201 cm^{-1}. One division of the *y*-axis in panel a corresponds to 0.008 absorbance unit. (b) The blue curve is the double-difference spectrum obtained from the data in panel a in the 1800−1000 cm^{-1} region, where the dotted line was subtracted from the solid one and multiplied by 2. The green curve is the difference spectrum between the Cl^--bound form and the Cl^--free form in the 1800−1000 cm^{-1} region (same as Figure 2). One division of the *y*-axis in panel b corresponds to 0.004 absorbance unit.

The solid and dotted lines in Figure 4a are essentially similar to each other. Both solid and dotted lines exhibit a negative ethylenic C═C stretch at 1543 cm^{-1}, negative fingerprint vibrations at 1237, 1201, and 1161 cm^{-1}, and a positive carboxylic C═O stretch at 1765 cm^{-1}, which are all characteristic of the M minus *p*pR difference spectrum (*30, 40*). However, there are some spectral alterations. A positive band appears at 1191 cm^{-1} only in the presence of Cl^-. Since this frequency is characteristic of the 13-*cis* form, an N-like intermediate containing protonated 13-*cis*-retinal may be formed in the presence of Cl^- (*41*). It should be noted that the N-like species was never observed for a hydrated film without salt (*30*). However, this contribution is not significant as is seen from small positive ethylenic C═C stretching vibrations at ∼1530 cm^{-1} for the solid line. Another difference is that the intensity of the positive 1765 cm^{-1} band is smaller in the presence of Cl^- than in the absence.

While the differences in the bands at 1191 and 1765 cm^{-1} are in the intensities, a remarkable shape difference was seen for the band at 1724 cm^{-1}. The negative band at 1724 cm^{-1} was observed for only the difference spectrum in the presence of Cl^-. A similar negative band at 1724 cm^{-1} was also reported by the previous time-resolved FTIR measurement (*42*). The frequency coincides with that of the C═O stretch of Asp193 (Figure 2), suggesting that Asp193 is deprotonated in the M state. Iwamoto et al. reported that the pK_a of PRG is 6.4 in *p*pR but drops to 4.9 in *p*pR_M in the presence of 400 mM NaCl, whereas the fast proton release does not occur in the absence of NaCl (*26*). This ATR-FTIR observation is fully consistent with their reports and identifies the PRG of *p*pR as Asp193.

The blue spectrum in Figure 4b represents the difference between the light-induced changes without Cl^- (dotted line in Figure 4a) and with Cl^- (solid line in Figure 4a), which was expanded by factor 2 to clearly show the peaks. Interestingly, the double-difference spectrum looks like a mirror image of that of binding of Cl^- to *p*pR (green spectrum in Figure 4b reproduced from Figure 2d). In fact, the peaks of the blue spectrum at 1724 (−), 1686 (+), 1671 (−), 1652 (+), 1619 (−), 1593 (+), 1542 (−), and 1526 (+) cm^{-1} are seen in the green spectrum with the opposite sign, though there are some exceptions, such as the bands at

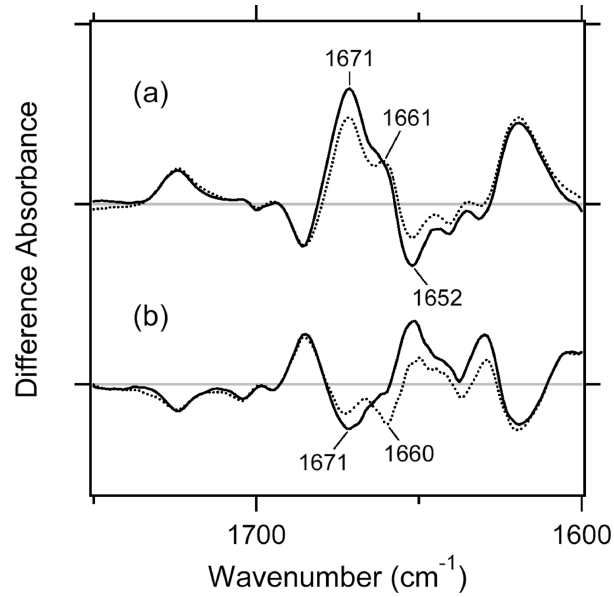

FIGURE 5: (a) Difference infrared spectra between the Cl^--bound form and the Cl^--free form by ATR-FTIR spectroscopy at 293 K in the 1750−1600 cm^{-1} region. The negative side represents the Cl^--free form, and the positive side represents the Cl^--bound form. Solid and dotted lines represent the spectra for the unlabeled and [^{15}N]arginine-labeled *p*pR, respectively. One division of the *y*-axis corresponds to 0.0025 absorbance unit. (b) Double-difference spectra obtained from the data of Figure 4a in the 1800−1000 cm^{-1} region, where the dotted line was subtracted from the solid one. Solid and dotted lines represent the spectra for unlabeled and [^{15}N]arginine-labeled *p*pR, respectively.

1765 (−) and 1191 (+) cm^{-1}. This fact implies that the M minus *p*pR difference spectrum in the presence of Cl^- can be divided into the two components reflecting two different processes: (i) the transfer of the proton from the Schiff base to Asp75 and (ii) the release of the proton from Asp193 to the aqueous phase. The former can be described by the M minus *p*pR difference spectrum in the absence of Cl^- (dotted line in Figure 4a), while the latter is described by the mirror image of the difference spectrum of Cl^- binding (Figure 2d). This further implies that the proton release accompanies the release of Cl^- in ppR_M.

Structural Changes of Arginine Residues in Chloride Binding and Dissociation. Figure 5a compares the difference spectra of Cl^- binding between unlabeled (solid lines) and [^{15}N]arginine-labeled (dotted lines) *p*pR in the 1750−1600 cm^{-1} region. It is obvious that the positive 1671 cm^{-1} band loses the intensity upon labeling of arginine, presumably because of the frequency downshift. This indicates that the band at 1671 cm^{-1} in *p*pR(Cl^-) contains a C═N stretching vibration of arginine. The negative 1652 cm^{-1} band also loses the intensity upon labeling of arginine (Figure 5a), which could be identified as the C═N stretching vibration of arginine in the Cl^--free form of *p*pR. An alternative interpretation is that the intensity loss of the negative 1652 cm^{-1} band is caused by the spectral downshift of the positive 1671 cm^{-1} band by 20−25 cm^{-1}. If the C═N stretching vibration has no coupling with other vibrations, the calculated isotope shift is 26 cm^{-1} (from 1671 to 1645 cm^{-1}). Coupling to other vibrational modes often results in smaller isotope shifts as observed here.

The solid line in Figure 5b shows the double-difference spectrum of the M minus *p*pR spectrum in the presence and absence of Cl^-, reproduced from Figure 4b (blue curve). The dotted line in Figure 5b shows the same double-difference spectrum, but for [^{15}N]arginine-labeled *p*pR. The negative 1671 cm^{-1} band exhibits an isotope shift to 1660 cm^{-1} by [^{15}N]arginine labeling, indicating that the 1671 cm^{-1} band contains the C═N stretching of arginine. The result also indicates the observed frequency shift to be 11 cm^{-1}. On the other hand, it is not clear if the positive bands in Figure 5b contain vibrations of arginine. It should be noted, however, that the spectra in panels a and b of Figure 5 both show isotope-induced spectral differences at 1680−1630 cm^{-1}, and the deviation between the solid and dotted lines at 1640−1630 cm^{-1} in Figure 5b cannot be explained by the negative peaks at 1671 (solid line) and 1660 cm^{-1} (dotted line). Thus, we infer that the bands at 1652 cm^{-1} in Figure 5a,b contain the C═N stretching mode of arginine as well, though the intensity is smaller. Thus, we assume the C═N stretching vibration of arginine to be at 1671 cm^{-1} in *p*pR(Cl^-) and at 1652 cm^{-1} in *p*pR(free) and ppR_M. According to the X-ray crystal structure of *p*pR (*28*), a Cl^- ion is coordinated to Arg72 which is connected to the Schiff base region. Since Arg72 is the only arginine residue in the transmembrane region, the band probably originates from Arg72.

DISCUSSION

Binding of Chloride to ppR. Iwamoto et al. reported that the fast release of the proton from ppR_M at pH 5−8 was diminished in the absence of Cl^- (*26*), suggesting that Cl^- binding controls the pK_a of the proton release group (PRG) in *p*pR and ppR_M. The X-ray crystal structure showed the Cl^- binding site being located near the extracellular surface (*28*). In this paper, we studied the Cl^--dependent proton release mechanism of *p*pR by means of ATR-FTIR spectroscopy. From the spectral analysis of Cl^- binding, protonation of a carboxylic acid was found upon binding of Cl^- to *p*pR. Since the C═O stretch was shifted from 1724 to 1705 cm^{-1} in the D193E mutant (Figure 3), we assigned the carboxylic acid as Asp193. This result shows the pK_a of Asp193 being increased by binding of Cl^- to *p*pR, where the negative charge of Cl^- electrostatically stabilizes the protonated state of Asp193.

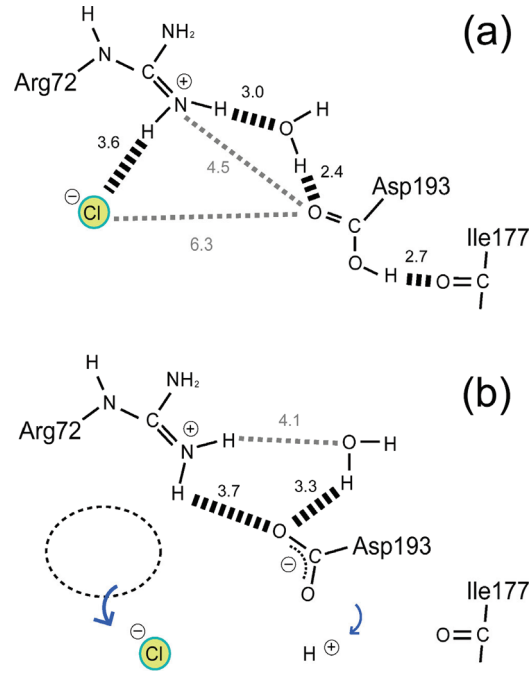

FIGURE 6: Schematic drawing of the proton release mechanism of *p*pR, which illustrates the vicinity of the Cl^- binding site in the extracellular region. (a and b) Structures of *p*pR and ppR_M, respectively, which coincide with those of *p*pR(Cl^-) (*28*) and *p*pR(free) (*27*). Numbers in the figures show the distances among nitrogen, oxygen, and Cl^- in angstroms, with the hydrogen atoms not taken into the account. In the presence of Cl^-, Asp193 is protonated in the unphotolyzed state (a), which is stabilized by two hydrogen bonds. In ppR_M, release of Cl^- and deprotonation of Asp193 take place, which also accompanies removal of an intervening water molecule between Arg72 and Asp193.

The X-ray structure of *p*pR(Cl^-) reported that the distances from Cl^- to the nearest nitrogen of Arg72 and the nearest oxygen of Asp193 (Figure 6) are 3.6 and 6.3 Å, respectively, suggesting that there is no direct contact between Cl^- and Asp193 (*28*). Therefore, the hydrogen bonding network presumably controls the pK_a of Asp193 and the K_d of Cl^-. The distance between Arg72 and Asp193 is 4.5 Å, and a water molecule is located between Arg72 and Asp193, at distances of 3.0 and 2.4 Å, respectively (*28*). Thus, a side chain oxygen of Asp193 is a hydrogen bond acceptor of the water. In addition, another side chain oxygen donates a hydrogen bond with the peptide carbonyl oxygen of Ile177, located 2.7 Å away. In the X-ray structure of *p*pR(free), the distance between Arg72 and Asp193 is reduced to 3.7 Å, so that the intervening water molecule is removed and Arg72 and Asp193 can interact directly (*27*). The peptide carbonyl of Ile177 is moved away (>4 Å) from Asp193. In the Cl^--

free form, these hydrogen bonding alterations stabilize negatively charged Asp193 (Figure 6).

The *p*pR(Cl^-) minus *p*pR(free) spectrum shows several sharp peaks (Figure 2d), among which the positive 1724 cm^{-1} band originates from protonation of Asp193. The 1671 (+)/1652 (−) cm^{-1} bands involve the C=N stretching vibration of Arg72 (Figure 5a). From the X-ray structure, the distance from Arg72 to either negative charge is almost the same, 3.6 Å to Cl^- in *p*pR(Cl^-) and 3.7 Å to an oxygen of Asp193 in *p*pR(free). On the other hand, the frequency change suggests a local environmental change of Arg72, and from the frequency, the positive charge appears to be more delocalized in the free form. A negative band at 1652 cm^{-1} may involve amide I vibration of an α-helix, suggesting that *p*pR(free) possesses higher α-helical content than *p*pR(Cl^-).

The peak at 1619 cm^{-1} is also noteworthy, as it has the characteristic frequency of β-sheet. The structures of *p*pR(Cl^-) (*28*) and *p*pR(free) (*27*) both have only one β-sheet in the B−C loop, from Trp60 to Phe69. On the other hand, a Cl^- binds to the bottom of the C helix (Figure 1b), where the Cl^- binding pocket is comprised by the side chains of Phe69 of β-sheet and Arg72 and Tyr73 of the C helix. Therefore, it is possible that the binding of Cl^- to *p*pR alters the β-sheet structure of the B−C loop. Interestingly, *p*pR(Cl^-) possesses a perfect antiparallel β-sheet from Trp60 to Phe69 (*28*), whereas the turn region of the β-sheet is loosened in *p*pR(free) (*27*). Consequently, one hydrogen bond in the β-sheet is lost in *p*pR(free) compared with that in *p*pR(Cl^-). Thus, an enhanced amide I vibration at 1619 cm^{-1} upon Cl^- binding is fully consistent with the two X-ray crystallographic structures.

Release of Chloride and Proton upon Formation of ppR_M. Figure 4a shows a negative peak at 1724 cm^{-1} only for *p*pR(Cl^-), not for *p*pR(free). This suggests that the formation of *p*pR_M accompanies deprotonation of Asp193, presumably leading to the release of a proton to the extracellular aqueous phase. This is consistent with the results of Iwamoto et al. which showed that the proton release occurs only in the presence of Cl^- (*26*). To unequivocally identify the negative 1724 cm^{-1} band in the *p*pR_M(Cl^-) minus *p*pR(Cl^-) spectrum (solid line in Figure 4a), we measured the spectra for D193E. Although protonation of Glu193 was observed at 1705 cm^{-1} upon Cl^- binding (Figure 3), the difference spectrum between the M and unphotolyzed states did not show a negative peak at 1705 cm^{-1} (data not shown). Nevertheless, this is also consistent with the results of Iwamoto et al., because they did not observe fast release of a proton from D193E. It is likely that the pK_a decrease does not occur in *p*pR_M of D193E, while the pK_a drops from 6.4 (*p*pR) to 4.9 (*p*pR_M) for the wild type. This fact suggests the important role of the hydrogen bonding network at the extracellular domain, where the machinery of the pK_a decrease in *p*pR_M is broken by the D-to-E mutation at position 193. Similar Cl^--dependent proton release was reported for D85T mutant BR that functions as a light-driven Cl^- pump (*43*).

The *p*pR_M minus *p*pR spectra are similar in the presence and absence of Cl^- (solid and dotted lines in Figure 4a). Nevertheless, the difference between them (blue curve in Figure 4b) resembles a mirror image of the spectrum of Cl^- binding to *p*pR (green curve in Figure 4b). A similar observation was reported for *pharaonis* halorhodopsin (*p*HR), where the light-induced O minus *p*HR spectrum resembles a mirror image of the spectrum of binding of Cl^- to *p*HR (*33*). This was interpreted in terms of the structural similarity between the O intermediate and the Cl^--free state of *p*HR. It should be noted that in this case, the light-induced M minus *p*pR spectrum does not resemble a mirror image of the spectrum of Cl^- binding to *p*pR, but the double-difference spectrum does. This suggests that structural changes in *p*pR_M can be essentially divided into the two domains, those at the extracellular surface and elsewhere. It is likely that in the presence of Cl^-, additional structural changes take place near the Cl^- binding site, leading to the release of Cl^- and a proton.

The trigger of the release of Cl^- and a proton is the formation of *p*pR_M by the transfer of a proton from the Schiff base to Asp75. How is such information conducted to the extracellular surface? One possibility is that an early event such as photoisomerization and transfer of a proton to Asp75 cause displacement of the C helix, leading to the Cl^- binding site and Asp193 being exposed to the aqueous phase. The 1665 (−)/1643 (+) cm^{-1} bands in the *p*pR_M minus *p*pR spectra (Figure 4a) implicate perturbation of an α-helix regardless of the presence of Cl^-, and appearance of a positive band at 1652 cm^{-1} in the blue spectrum of Figure 4b suggests stabilization of an α-helix. A negative 1619 cm^{-1} band in the blue spectrum of Figure 4b also suggests destabilization of the β-sheet. These secondary structure alterations must be correlated with the release of Cl^- and a proton from the extracellular domain of *p*pR.

The intraprotein hydrogen bonding network probably participates in the pK_a change of Asp193, where Arg72 plays a crucial role. In fact, we observed the frequency change of the 1671 cm^{-1} band, the characteristic frequency of the C=N stretching vibration of arginine (*44*), that most likely can be ascribed to Arg72 (Figure 5). It should be noted that the M minus *p*pR difference spectra in the absence of Cl^- did not exhibit an isotope shift of [^{15}N]arginine (data not shown), suggesting that Arg72 interacts with the deprotonated Asp193 in both *p*pR and *p*pR_M. In the case of BR, downward motion of the side chain of Arg82 to the extracellular side has been reported (*45*). The orientation of the side chain of Arg72 is similar between *p*pR(Cl^-) and *p*pR(free) (Figure 1), and these results strongly suggest that this orientation in *p*pR_M is similar to that in *p*pR(free). If it is the case, no orientation change may take place for Arg72. Nevertheless, hydrogen bonding interactions of Arg72 are considerably altered between *p*pR(Cl^-) and *p*pR(free) (Figure 6), which is strongly correlated with the release of Cl^- and a proton in *p*pR_M.

In summary, this ATR-FTIR spectroscopic study of *p*pR revealed that binding of Cl^- to *p*pR accompanies protonation of Asp193. Light-induced *p*pR_M minus *p*pR difference ATR-FTIR spectra show the deprotonation signal of Asp193 (at 1724 cm^{-1}) only in the presence of Cl^-. The double-difference spectrum between the light-induced changes in the presence and absence of Cl^- is a mirror image of that of Cl^- binding in the dark, indicating that *p*pR_M formation is accompanied by simultaneous deprotonation of Asp193 and dissociation of Cl^-. Structural changes of an arginine, probably Arg72, are involved in

these processes together with secondary structure alterations of an α-helix and the β-sheet. It is thus concluded that the PRG of *p*pR includes Asp193, whose pK_a changes are controlled by Cl^- and Arg72.

ACKNOWLEDGMENT

We thank Dr. Masayuki Iwamoto for invaluable discussion and Dr. Leonid S. Brown for helpful comments.

REFERENCES

1. Haupts, U., Tittor, J., and Oesterhelt, D. (1999) Closing in on bacteriorhodopsin: Progress in understanding the molecules. *Annu. Rev. Biophys. Biomol. Struct. 28*, 367–399.
2. Lanyi, J. K. (2004) Bacteriorhodopsin. *Annu. Rev. Physiol. 66*, 665–688.
3. Kandori, H. (2000) Role of internal water molecules in bacteriorhodopsin. *Biochim. Biophys. Acta 1460*, 177–191.
4. Kandori, H. (2004) Hydration switch model for the proton transfer in the Schiff base region of bacteriorhodopsin. *Biochim. Biophys. Acta 1658*, 72–79.
5. Tanimoto, T., Furutani, Y., and Kandori, H. (2003) Structural changes of water in the Schiff base region of bacteriorhodopsin: Proposal of a hydration switch model. *Biochemistry 42*, 2300–2306.
6. Zimányi, L., Váró, G., Chang, M., Ni, B., Needleman, R., and Lanyi, J. K. (1992) Pathways of proton release in the bacteriorhodopsin photocycle. *Biochemistry 31*, 8535–8543.
7. Brown, L. S., Sasaki, J., Kandori, H., Maeda, A., Needleman, R., and Lanyi, L. J. (1995) Glutamic acid 204 is the terminal proton release group at the extracellular surface of bacteriorhodopsin. *J. Biol. Chem. 270*, 27122–27126.
8. Balashov, S. P., Imasheva, E. S., Ebrey, T. G., Chen, N., Menick, D. R., and Crouch, R. K. (1997) Glutamate-194 to cysteine mutation inhibits fast light-induced proton release in bacteriorhodopsin. *Biochemistry 36*, 8671–8676.
9. Dioumaev, A. K., Richter, H.-T., Brown, L. S., Tanio, M., Tuzi, S., Saito, H., Kimura, Y., Needleman, R., and Lanyi, J. K. (1998) Existence of a proton transfer chain in bacteriorhodopsin: Participation of Glu-194 in the release of protons to the extracellular surface. *Biochemistry 37*, 2496–2506.
10. Rammelsberg, R., Huhn, G., Lubben, M., and Gerwert, K. (1998) Bacteriorhodopsin's intramolecular proton-release pathway consists of a hydrogen-bonded network. *Biochemistry 37*, 5001–5009.
11. Zscherp, C., Schlesinger, R., Tittor, J., Oesterhelt, D., and Heberle, J. (1999) In situ determination of transient pK_a changes of internal amino acids of bacteriorhodopsin by using time-resolved attenuated total reflection Fourier-transform infrared spectroscopy. *Proc. Natl. Acad. Sci. U.S.A. 96*, 5498–5503.
12. Zscherp, C., Schlesinger, R., and Heberle, J. (2001) Time-resolved FT-IR spectroscopic investigation of the pH-dependent proton transfer reactions in the E194Q mutant of bacteriorhodopsin. *Biochem. Biophys. Res. Commun. 283*, 57–63.
13. Garczarek, F., Wang, J., EI-Sayed, M. A., and Gerwet, K. (2004) The assignment of the different infrared continuum absorbance changes observed in the 3000−1800 cm^{-1} region during the bacteriorhodopsin photocycle. *Biophys. J. 87*, 2676–2682.
14. Garczarek, F., Brown, L. S., Lanyi, J. K., and Gerwert, K. (2005) Proton binding within a membrane protein by a protonated water cluster. *Proc. Natl. Acad. Sci. U.S.A. 102*, 3633–3638.
15. Garczarek, F., and Gerwert, K. (2005) Functional waters in intraprotein proton transfer monitored by FTIR difference spectroscopy. *Nature 439*, 109–112.
16. Lórenz-Fonfría, V. A., Furutani, Y., and Kandori, H. (2008) Active internal waters in the bacteriorhodopsin photocycle. A comparative study of the L and M intermediates at room and cryogenic temperatures by infrared spectroscopy. *Biochemistry 47*, 4071–4081.
17. Krebs, M. P., and Khorana, H. G. (1993) Mechanism of light-dependent proton translocation by bacteriorhodopsin. *J. Bacteriol. 175*, 1555–1560.
18. Balashov, S. P. (2000) Protonation reactions and their coupling in bacteriorhodopsin. *Biochim. Biophys. Acta 1460*, 75–94.
19. Dioumaev, A. K., Brown, L. S., Shih, J., Spudich, E. N., Spudich, J. L., and Lanyi, J. K. (2002) Proton transfers in the photochemical reaction cycle of proteorhodopsin. *Biochemistry 41*, 5348–5358.
20. Waschuk, S. A., Bezerra, A. G., Jr., Shi, L., and Brown, L. S. (2005) *Leptosphaeria* rhodopsin: Bacteriorhodopsin-like proton pump from a eukaryote. *Proc. Natl. Acad. Sci. U.S.A. 102*, 6879–6883.
21. Kamo, N., Shimono, K., Iwamoto, M., and Sudo, Y. (2001) Photochemistry and photoinduced proton-transfer by *pharaonis* phoborhodopsin. *Biochemistry (Moscow, Russ. Fed.) 66*, 1277–1282.
22. Spudich, J. L., and Luecke, H. (2002) Sensory rhodopsin II: Functional insights from structure. *Curr. Opin. Struct. Biol. 12*, 540–546.
23. Gordeliy, V. I., Labahn, J., Moukhametzianov, R., Efremov, R., Granzin, J., Schlesinger, R., Büldt, G., Savopol, T., Scheidig, A. J., Klare, J. P., and Engelhard, M. (2002) Molecular basis of transmembrane signalling by sensory rhodopsin II-transducer complex. *Nature 419*, 484–487.
24. Schmies, G., Lüttenberg, B., Chizhov, I., Engelhard, M., Becker, A., and Bamberg, E. (2000) Sensory rhodopsin II from the *haloalkaliphilic natronobacterium pharaonis*: light-activated proton transfer reactions. *Biophys. J. 78*, 967–976.
25. Sudo, Y., Iwamoto, M., Shimono, K., Sumi, M., and Kamo, N. (2001) Photo-induced proton transport of *pharaonis* phoborhodopsin (sensory rhodopsin II) is ceased by association with the transducer. *Biophys. J. 80*, 916–922.
26. Iwamoto, M., Hasegawa, C., Sudo, Y., Shimono, K., Araiso, T., and Kamo, N. (2004) Proton release and uptake of *pharaonis* phoborhodopsin (sensory rhodopsin II) reconstituted into phospholipids. *Biochemistry 43*, 3195–3203.
27. Luecke, H., Schobert, B., Lanyi, J. K., Spudich, E. N., and Spudich, J. L. (2001) Crystal structure of sensory rhodopsin II at 2.4 angstroms: Insights into color tuning and transducer interaction. *Science 293*, 1499–1503.
28. Royant, A., Nollert, P., Edman, K., Neutze, R., Landau, E. M., Pebay-Peyroula, E., and Navarro, J. (2001) X-ray structure of sensory rhodopsin II at 2.1 Å resolution. *Proc. Natl. Acad. Sci. U.S.A. 98*, 10131–10136.
29. Kandori, H., Shimono, K., Sudo, Y., Iwamoto, M., Shichida, Y., and Kamo, N. (2001) Structural changes of *pharaonis* phoborhodopsin upon photoisomerization of the retinal chromophore: Infrared spectral comparison with bacteriorhodopsin. *Biochemistry 40*, 9238–9246.
30. Furutani, Y., Iwamoto, M., Shimono, K., Kamo, N., and Kandori, H. (2002) FTIR spectroscopy of the M photointermediate in *pharaonis* phoborhodopsin. *Biophys. J. 83*, 3482–3489.
31. Furutani, Y., Sudo, Y., Kamo, N., and Kandori, H. (2003) FTIR spectroscopy of the complex between *pharaonis* phoborhodopsin and its transducer protein. *Biochemistry 42*, 4837–4842.
32. Furutani, Y., Kamada, K., Sudo, Y., Shimono, K., Kamo, N., and Kandori, H. (2005) Structural changes of the complex between *pharaonis* phoborhodopsin and its cognate transducer upon formation of the M photointermediate. *Biochemistry 44*, 2909–2915.
33. Guijarro, J., Engelhard, M., and Siebert, F. (2006) Anion uptake in halorhodopsin from *Natromonas pharaonis* studied by FTIR spectroscopy: Consequences for the anion transport mechanism. *Biochemistry 45*, 11578–11588.
34. Iwaki, M., Puustinen, A., Wikström, M., and Rich, P. R. (2003) ATR-FTIR spectroscopy of the P_M and F intermediates of bovine and *Paracoccus denitrificans* cytochrome *c* oxidase. *Biochemistry 42*, 8809–8817.
35. Iwaki, M., Cotton, N. P., Quirk, P. G., Rich, P. R., and Jackson, J. B. (2006) Molecular recognition between protein and nicotinamide dinucleotide in intact, proton-translocating transhydrogenase studied by ATR-FTIR Spectroscopy. *J. Am. Chem. Soc. 128*, 2621–2629.
36. Jiang, X., Zaitseva, E., Schmidt, M., Siebert, F., Engelhard, M., Schlesinger, R., Ataka, K., Vogel, R., and Heberle, J. (2008) Resolving voltage-dependent structural changes of a membrane photoreceptor by surface-enhanced IR difference spectroscopy. *Proc. Natl. Acad. Sci. U.S.A. 105*, 12113–12117.
37. Shimono, K., Ikeura, Y., Sudo, Y., Iwamoto, M., and Kamo, N. (2001) Environment around the chromophore in *pharaonis* phoborhodopsin: Mutation analysis of the retinal binding site. *Biochim. Biophys. Acta 1515*, 92–100.
38. Tanimoto, T., Shibata, M., Belenky, M., Herzfeld, J., and Kandori, H. (2004) Altered hydrogen bonding of Arg82 during the proton pump cycle of bacteriorhodopsin: A low-temperature polarized FTIR spectroscopic study. *Biochemistry 43*, 9439–9447.
39. Shimono, K., Kitami, M., Iwamoto, M., and Kamo, N. (2000) Involvement of two groups in reversal of the bathochromic shift

of *pharaonis* phoborhodopsin by chloride at low pH. *Biophys. Chem. 87*, 225–230.

40. Engelhard, M., Scharf, B., and Siebert, F. (1996) Protonation changes during the photocycle of sensory rhodopsin II from *Natronobacterium pharaonis*. *FEBS Lett. 395*, 195–198.
41. Pfefferlé, J. M., Maeda, A., Sasaki, J., and Yoshizawa, T. (1991) Fourier transform infrared study of the N intermediate of bacteriorhodopsin. *Biochemistry 30*, 6548–6556.
42. Bergo, V., Spudich, E. N., Spudich, J. L., and Rothschild, K. J. (2003) Conformational changes detected in a sensory rhodopsin II-transducer complex. *J. Biol. Chem. 278*, 36556–36562.
43. Brown, L. S., Needleman, R., and Lanyi, J. K. (1996) Interaction of proton and chloride transfer pathways in recombinant bacteriorhodopsin with chloride transport activity: Implications for the chloride translocation mechanism. *Biochemistry 35*, 16048–16054.
44. Kötting, C., Kallenbach, A., Suveyzdis, Y., Wittinghofer, A., and Gerwert, K. (2008) The GAP arginine finger movement into the catalytic site of Ras increases the activation entropy. *Proc. Natl. Acad. Sci. U.S.A. 105*, 6260–6265.
45. Luecke, H., Schobert, B., Richter, H. T., Cartailler, J. P., and Lanyi, J. K. (1999) Structural changes in bacteriorhodopsin during ion transport at 2 angstrom resolution. *Science 286*, 255–260.
46. Shimono, K., Furutani, Y., Kamo, N., and Kandori, H. (2003) Vibrational modes of the protonated Schiff base in *pharaonis* phoborhodopsin. *Biochemistry 42*, 7801–7806.
47. Kandori, H., Furutani, Y., Shimono, K., Shichida, Y., and Kamo, N. (2001) Internal water molecules of *pharaonis* phoborhodopsin studied by low-temperature infrared spectroscopy. *Biochemistry 40*, 15693–15698.

BI801984U